Creaming of emulsions: the role of depletion forces induced by surfactant

J. Bibette, D. Roux, B. Pouligny

Classification
Physics Abstracts
05.70 F — 64.70 D — 82.70 K

Creaming of emulsions: the role of depletion forces induced by surfactant

J. Bibette, D. Roux and B. Pouligny

Centre de Recherche Paul Pascal, C.N.R.S., Avenue A. Schweitzer, 33600 Pessac, France

(Received 13 May 1991, revised 22 October 1991, accepted 27 November 1991)

Abstract. — We show that excess surfactant, or salt, in the bulk phase of an oil in water ionic emulsion has strong consequences on the thermodynamical behavior of the dispersion. Static light scattering experiments have been performed to investigate the attractive interaction induced by micelles according to a depletion mechanism. This interaction can be largely reduced by adding salt. This depletion interaction leads to a phase transition which is characterized as a fluid-solid transition. The long range ordering of the droplets dense phase is characterized by visible light diffraction. The experimental phase diagram is quantitatively analysed as a transition between a perfect gaz and a harmonic solid. An analytical model is worked out from which we analyze the general phase diagram in terms of the volume fraction of the droplets, of the depth of their interaction potential and of the ratio (δ/σ), where δ is the range of the interaction and σ the droplet diameter. Cuts of the phase diagram at constant (δ/σ) feature a liquid-gas or a liquid-solid transition.

1. Introduction.

Emulsions are three-component mixtures of oil, water, and surfactant. Their structure can be described as spherical droplets covered with surfactant and dispersed in a continuous phase (solvent). Both oil-in-water and water-in-oil emulsions are encountered [1, 2]. Emulsions are of considerable industrial importance in a broad range of applications such as cosmetology, food industry, lubrication and paint industry. In all cases, emulsion technology is a mean to make homogeneous a mixture of oil and water. Emulsions allow also to avoid organic solvents, what is one of the main property which is widely used in industrial areas such as lubrication or paint.

Thermodynamically speaking, the emulsions are metastable systems which means that they are prepared using an excess energy (mechanical in most cases). After a period of time which depends strongly on the preparation method, the surfactant and oil properties, the emulsion eventually phase separates in two phases: a water plus surfactant phase and the organic phase. The phase separation process involves coalescence of the droplets which grow as a function of

time, this is an irreversible process. To come back to the original stage (emulsion), energy has to be furnished to the system. The characteristic time of coalescence can vary tremendously, depending upon the systems. In certain cases, this time can be extremely long and no coalescence happens for years, making this kind of emulsions kinetically "stable". Thus, one can consider these emulsions as colloidal suspensions of spheres without worrying much about the coalescence process. However, due to the non-equilibrium nature of the phase, the average droplet size is not only a function of the system studied but also of the preparation way. Usually the polydispersity is large and depends also on the preparation scheme. In the following, we will restrict ourselves to systems which do not exhibit coalescence and consequently can be considered as regular colloidal suspensions.

Besides the coalescence process, emulsions often exhibit an other type of destabilization. In certain cases, flocculation may occur as for regular colloidal systems and depending upon the respective density of the solvent and the droplets, sedimentation or creaming occurs. Indeed, the droplets aggregate, without coalescing, and the aggregates separate from the bulk. Creaming happens when the droplets density is lower than the solvent density (oil-in-water systems) and sedimentation happens in the opposite case (water-in-oil). The role of the emulsifier (surfactant) in causing flocculation has been first recognized by Cockbain [3] in 1952 but neither his nor other work following his pioneering remarks offered a plausible explanation [4]. It is quite recently that an explanation has been proposed to account for the flocculation: indeed Fairhurst *et al.* [5] and Aronson [6] have proposed that flocculation arises from depletion of non adsorbed surfactant making micelles. This is similar to the well known destabilization of colloids by non-adsorbing polymers [7,11]. The same mechanism was also proposed to account for flocculation of polystyrene latex by surfactant [12].

Depletion interactions arise in a colloidal system of interacting spheres when the solvent contains a characteristic length (ξ) which is excluded from the volume comprised between two approaching spheres at distance d ($d < \xi$). This mechanism leads to attractive effective interaction between the spheres and is in certain cases responsible for flocculation. The first theoretical description of such a mechanism was proposed by Asakura *et al.* [7] for a bimodal distribution of hard spheres.

This mechanism has also been applied by Vrij [8] and Joanny *et al.* [9] to colloidal suspensions in a polymer solution leading to analytical expressions for the depletion pair potential between colloidal particles. More recently, De Gennes *et al.* [13] have proposed that a similar interaction can occur between colloidal particles imbedded in a binary critical fluid. A Percus Yevick calculation leads also to effective attractive interactions when two sizes of particles are taken into account [14]. This phenomenon exists also in non isotropic liquid [15]. Let us point out that it is a very general process that is entropic in origin. This comes from the fact that the bulk entropy is increased when two colloidal particles approach as long as the distance between the two surfaces of the particle is smaller than the correlation length of the fluctuations. Up to now besides a large amount of theoretical work there are only a few experimental evidence for the depletion mechanism [16, 17].

We present in this paper an experimental study of the effect of excess surfactant to the thermodynamical behavior of non coalescing emulsions (made of silicone oil, Sodium Dodecyl Sulfate and water). Due to the extreme slowing down of the coalescence process we can consider the emulsion studied as being at equilibrium and thermodynamical treatment can be applied to understand its behavior. Taking advantage of the creaming effect, we were able to prepare monodisperse emulsions [18]. This is the key point for a clean comparison with theories.

The paper is organized as follows. In part 2 the emulsion droplets-SDS-water-NaCl quaternary phase diagram is presented and evidences for a liquid solid phase transition are given using direct phase contrast microscopic observations.

In part 3, we introduce the light scattering experiments and we comment on the ability of the Rayleigh-Gans approximation to describe the angular dependence of the light scattered by emulsions like systems.

In part 4, we study the correlations between the oil droplets in the fluid phase using static light scattering experiments. Attractive interactions are measured originating in the presence of SDS micelles *via* a depletion mechanism.

In part 5, we investigate the structure of the dense phase. A colloidal crystal structure is demonstrated by visible light Bragg diffractions. Consequently we conclude that attractive forces drive a fluid-solid transition.

In part 6, we model the fluid-solid phase transition as a transition between a perfect gas and a harmonic solid. This very simple view is able to fit quantitatively experimental phase diagrams and predicts a universal logarithmic shape for any fluid-solid transition far from appearance conditions of a triple point.

Finally in part 7, the competition between fluid solid and liquid gas transition is discussed in terms of particles diameters compared to the range of the attractive potential. Then it is demonstrated that emulsions give only a fluid solid phase transition which has been considered up to now as flocculation because polydispersity masks the cristalline nature of aggregates.

2. Direct observations by optical microscopy and phase diagrams.

The stock emulsion studied has been prepared at Rhône-Poulenc Company Laboratory [19]. The technique used to make the stock emulsion is the classical inversion method [2]. The first step is to mix slowly during 15 mn aqueous emulsifier solution (5 g SDS, 10 g water) in 100 g silicone oil (SDS surfactant comes from Prolabo and silicone oil comes from Rhône-Poulenc). This first step leads to a water-in-oil emulsion with very large droplets ($>10\mu$m). This emulsion is then inverted to an oil-in-water emulsion using a colloidal mixer (Moritz BF 50). Finally this emulsion is diluted with pure water under mixing during a few minutes. The average droplets size may range from 0.2 to a few microns. Let first consider the behavior of a typical polydisperse emulsion (oil volume fraction $\Phi = 10\,\%$) upon SDS concentration changes. For low values of the SDS concentration (close to the cmc, cmc $= 8\times10^{-3}$ mol.l^{-1}), the emulsion is homogeneous (see Fig. 1a) whereas for higher surfactant concentration, roughly 0.05 mol.l^{-1}, oil droplets aggregate into clusters which coexist with free droplets (see Fig. 1b). With time these flocs separate from the dilute phase and form a cream on the top of the sample (silicone oil density is 0.94). Before the separation occurs due to gravity effect, the microscope observation clearly reveals a dynamical exchange between the free droplets and the ones trapped in the clusters. Moreover, if the cream which is the droplet rich phase, is diluted with water, one gets instantaneously an homogeneous emulsion showing that the transition is reversible. Note that during this process, as mentioned by Aronson [6] for different emulsions, there is no coalescence processes. This flocculation phenomenon can be used to produce monodisperse samples. Indeed, a careful observation indicates that very close to the transition threshold, the dense phase contains a majority of big droplets of the polydisperse emulsion. Therefore, the cream obtained after separation is richer in big droplets and the dilute phase is richer in small ones. Repeating this operation is a very efficient way of separating droplets of differents sizes [18]. A typical sample of a monodisperse emulsion (diameter $\sigma = 0.7\,\mu$m) extracted from the polydisperse one (1a) is shown in figure 2a. With such monodisperse systems, we will examine again the effect of adding surfactant. As previously described, adding surfactant leads to the formation of aggregates coexisting with free droplets (see Fig. 2b). Likewise, the two coexisting phases (dense: aggregates and dilute: free droplets) exchange continuously particles as it can

be observed under microscope. This strongly suggests the existence of a true thermodynamical equilibrium. Moreover the pure dense phase looks solid-like (see Fig. 3). Since we expect a true thermodynamical equilibrium, one can draw a phase diagram for various droplet sizes ($\sigma = 0.46\,\mu$m ; $\sigma = 0.60\,\mu$m ; $\sigma = 0.93\,\mu$m). First, we present phase diagrams in the surfactant concentration/oil volume fraction plane (Fig. 4a). The surfactant concentration is expressed as the volume fraction of SDS micelles (critical micellar concentration (cmc) = 8×10^{-3} mol^{-1} ; micellar diameter (σ_m) = 40 Å ; agregation number (ν) = 70). The limits between the one phase region where only free droplets are observed and the two-phase region where aggregated and free droplets coexist have been determined by observations under microscope. The so-called creaming effect is systematically observed at the macroscopic level when the surfactant concentration threshold is reached.

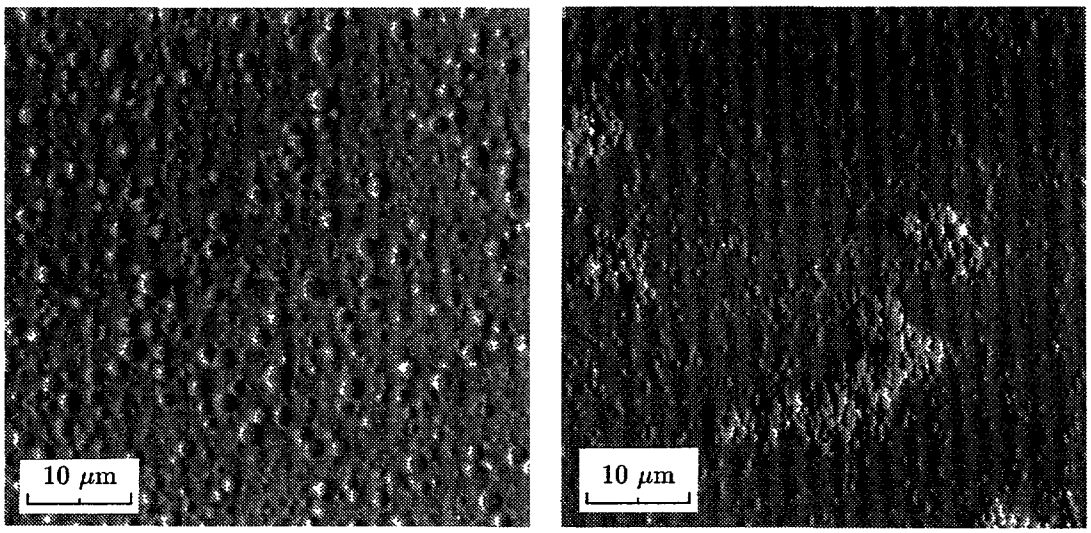

Fig. 1. — Pictures taken with an optical microscope using the differential interferential technique of Nomarsky: each droplet is delimited by a black and white crescent. Picture 1a shows a homogeneous polydisperse emulsion made of free droplets for an oil volume fraction equal to 10% and a bulk surfactant concentration equal to the cmc (cmc = 8×10^{-3} mol.l^{-1}). The 1b picture shows the effect of adding surfactant for the same oil volume fraction ($c = 5 \times 10^{-2}$ mol.l^{-1}) : flocs separate from a coexisting fluid phase.

Owing to the ionic nature of the surfactant (SDS), the effect of salt has also been investigated. Figure 4b presents phase diagrams for three selected samples. They are reported in the surfactant/salt concentration plane for two distinct fixed values of the oil volume fraction ($\Phi = 1\%$, $\Phi = 10\%$). There are two different regimes : for low salt concentration (C_{salt}<0.2 mol.l^{-1}), there is a reentrant fluid phase: the solid melts when salt is added. This effect is opposite to what is expected, since the salt is likely to decrease the electrostatic repulsion part of the pair potential and consequently should lead to a more attractive system stabilizing the solid phase. For higher values of the salt concentration (0.3 mol.l^{-1}) flocculation is observed, whatever the surfactant concentration. This transition is also reversible, but no

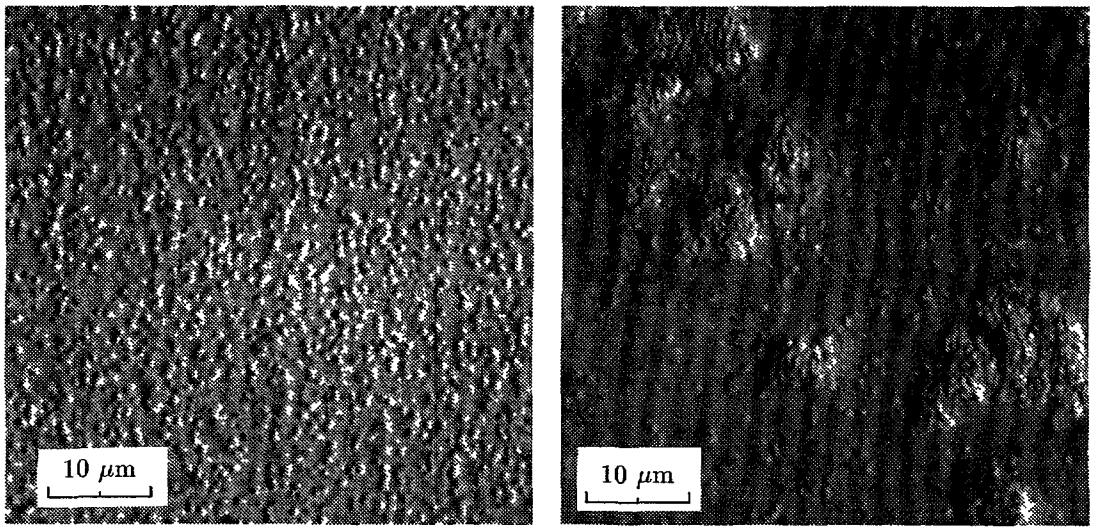

Fig. 2. — Picture 2a shows a monodisperse purified emulsion ($\Phi = 10\,\%$, C = cmc), the oil droplet diameter is 0.7 μm. This emulsion was extracted from the polydisperse one (Fig. 1a). Picture 2b shows again for the same monodisperse sample the effect of added surfactant: flocs and coexisting fluid are clearly visible ($C = 4 \times 10^{-2}$ mol.l^{-1}).

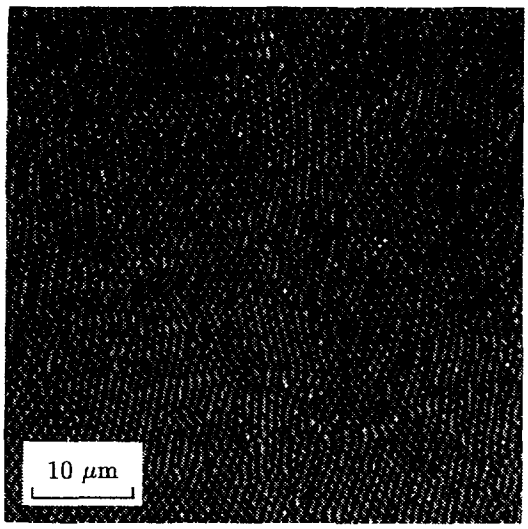

Fig. 3. — Picture showing the structure of the dense phase for $\sigma = 0.93\,\mu$m. The long range ordering of this phase is clearly visible.

solid-like structure of aggregates is observed due to a too fast kinetic phase transition driven by Van der Waals attractives forces [20].

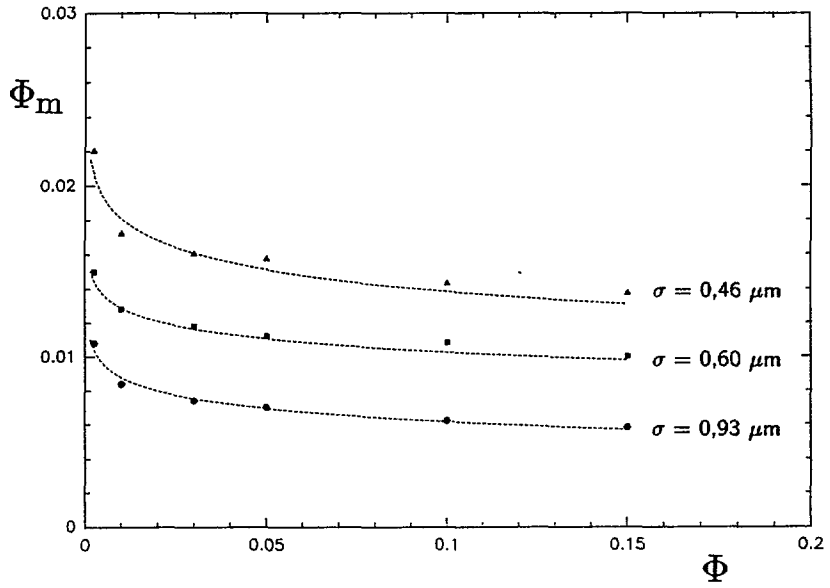

a)

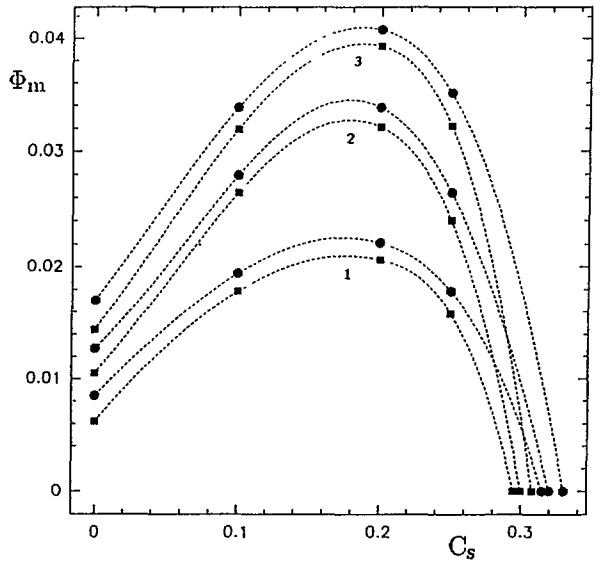

b)

Fig. 4. — a) Phase diagram in the micelle volume fraction/oil droplet volume fraction: (Φ_m/Φ) plane. The droplet sizes are 0.93 μm (•), 0.60 μm (■), 0.46 μm (▲). The dotted lines are theoretical predictions for the phase boundaries (see text below) and separate the one phase region (fluid) from the two phase region (fluid-solid). b) We report the phase diagram in the (Φ_m/C_s) plane where C_s is the salt concentration (NaCl) for two distinct values of the oil volume fraction Φ ((•): 1 %; (■): 10 %). Curves 1, 2, 3 correspond respectively to σ =0.93 μm; 0.6 μm and 0.46 μm and separate the upper two phase region from the bottom fluid phase region. Note the ability of salt to extend the fluid phase region.

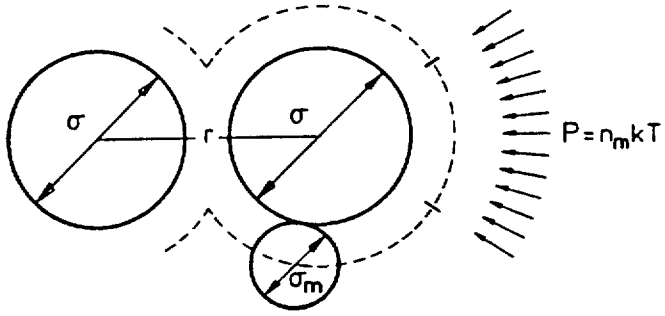

Fig. 5. — Kinetic approach for the depletion mechanism proposed by Vrij: when two large particles are close enough to each other, the region between them becomes inaccessible to the small ones. The osmotic pressure of the small particles drives the bigger ones closer together. Following Vrij, this osmotic pressure is taken to be the ideal gas one ($n_m kT$).

Attractive interactions must be evoked to explain consistently the phase diagram: indeed, the phase transition occurs at low volume fractions, which is possible only with attractive interactions in the absence of long range repulsive interaction (Debye length is of the order of 50 Å) [21].

One plausible attractive mechanism, already proposed [5,6] is a depletion interaction induced by surfactant micelles. The ideal gas approach developped by Vrij [8] is appropriate to describe the depletion mechanism: micelles are very small objects compared to oil droplets, and are always very dilute (micelle volume fraction $\Phi_m \simeq 1\,\%$). In other connections, resolutions of triplet correlation functions using Percus Yevik closure approximation [14] show a very good agreement with the Vrij assumption, as long as the volume fraction of small particles (micelles in our case) is less than 5 % and the dissymmetry in sizes remains of the order of ten. Let us recall the Vrij approach based on ideal gas kinetic theory (see Fig. 5): when two droplets come closer to each other than the micellar diameter (σ_m) , the inter droplet spacing becomes an excluded volume for micelles. This results in an attraction between colloids due to the non compensated pressure. Indeed, the pressure exerted is $n_m kT$ outside the excluded volume, where n_m is the micelle concentration, and is zero inside.

The Vrij assumption leads to the equation:

$$u(r) = -\frac{4\pi}{3} n_m\, kT\, \bar{\sigma}^3 \left(1 - \frac{3}{4}\frac{r}{\bar{\sigma}} + \frac{1}{16}\left(\frac{r}{\bar{\sigma}}\right)^3\right) \tag{2.1}$$

where $\bar{\sigma}$ is defined as $\bar{\sigma} = \dfrac{\sigma + \sigma_m}{2}$ r is the center to center separation distance between the particles.

Since the ratio $\dfrac{\sigma_m}{\sigma}$, in our case, is very small (10^{-2}), we can expand the Vrij equation with respect to the quantity $x = \dfrac{\sigma_m}{\sigma}$ and truncating the expansion at the third order, we get for the contact value potential:

$$u(\sigma) = -\frac{3}{2} kT\, \Phi_m \frac{\sigma}{\sigma_m} \tag{2.2}$$

This equation provides a simple linear dependance of the contact potential with the micelle volume fraction Φ_m and the ratio $\dfrac{\sigma}{\sigma_m}$ The range is always equal to σ_m. Qualitatively the

depletion mechanism described by equation (2.1) is consistent with phase diagrams shown in figure 4a. Indeed, higher Φ_m value are required as the droplet diameter is decreased to get the phase separation, what is suggested by equation (2.2).

Finally, note that our experimental phase diagram (Fig. 4a) compares qualitatively well with the one found by Vincent *et al.* [22] in a completely different system where depletion hypothesis is applied to account for flocculation induced by polymers in a non aqueous solvent. We will discuss further (Sect. 3) the salt effect responsible for the reentrant fluid phase appearance.

At this stage, we need the relationship between phase diagrams variables (surfactant concentration and salt concentration) and pair interactions between droplets. These informations have been obtained using the light scattering technique.

3. Static light scattering experiments and Rayleigh-Gans approximation for emulsion like systems.

We used light scattering (and diffraction) to investigate the correlations between the big droplets in the fluid phase, and the structure of the dense phase. Light scattering data are known to be easily interpretable only in the so-called "single-scattering regime". In this regime, each particle essentially senses the bare incident plane wave radiated by the light source. Secondary sources originating from the light scattered by the other particles are negligible.

We suppose that the sample is illuminated by a source of wave vector $\mathbf{k}_0$ and that the observation is made in the direction parallel to a vector $\mathbf{k}_S$, with $|\mathbf{k}_S| = |\mathbf{k}_0|$. The source is polarized perpendicularly to the plane defined by $\mathbf{k}_0$ and $\mathbf{k}_S$. In a medium composed of spheres, and in the single scattering regime, the intensity of the scattered light takes on the simple form:

$$I(\mathbf{q}) = P(\mathbf{q})\, S(\mathbf{q}) \tag{3.1}$$

with

$$\mathbf{q} = \mathbf{k}_S - \mathbf{k}_0 \tag{3.2}$$

$S(\mathbf{q})$, the so-called "structure factor", reflects the correlations between particles centers of mass and is given by [23]:

$$S(\mathbf{q}) = \sum_{\ell,m} \left\langle e^{i\mathbf{q}\cdot(\mathbf{r}_\ell - \mathbf{r}_m)} \right\rangle \tag{3.3}$$

where $\mathbf{r}_\ell$ and $\mathbf{r}_m$ are the positions of the centers of particles ℓ and m, respectively.

$P(\mathbf{q})$ is the "form factor". It depends on the size of the particle and on the refractive indices of both the particle (n_P) and of the solvant (n_S) around it.

Because the particles are spherical and the medium is isotropic on a macroscopic scale, $I(\mathbf{q})$, $P(\mathbf{q})$ and $S(\mathbf{q})$ depend only on the modulus of q, which is given by:

$$q = \frac{4\pi n_S}{\lambda} \sin\frac{\theta}{2} \tag{3.4}$$

λ is the wavelength of the light source in vacuum and θ is the angle betrween $\mathbf{k}_0$ and $\mathbf{k}_S$.

If the particle radius (a) or the difference $\Delta n = n_S - n_P$ are small enough, then $P(q)$ is just the squared modulus of the Fourier transform of a ball of radius a [24]:

$$P(q) = \left[\frac{3}{(qa)^3}(\sin qa - qa\cos qa)\right]^2 \tag{3.5}$$

Equation (3.5) is known as the Rayleigh-Gans (RG) approximation for the form factor of a sphere.

If the particles are large and if the contrast Δn is high, the RG approximation is expected to fail and the single scattering approximation as well. In practice, in definitely multiple scattering regimes, the way in which $I(q)$ varies as a function of q is known to be influenced by the sample and illuminated volume geometries. We used very small sample thicknesses, namely in the range 10-40 μm, and we checked that the shape of $I(q)$ *versus* q was constant in this range. This, we think, rules out the possibility of a strong multiple scattering contribution to the measured intensities. A rough criterion for the applicability of the RG approximation is

$$\sigma \cdot |\Delta n| \ll \lambda \tag{3.6}$$

The experimental orders of magnitude, $\Delta n \simeq 0.1$ and $\sigma \sim \lambda$ are neither definitely consistent nor definitely unconsistent with inequality (3.6). The only way to decide is to calculate the exact form factor directly from the Lorentz-Mie (LM) theory [25] and to compare with equation (3.5). Figure 6 shows the LM and RG form factors for $\sigma = 0.93\,\mu$m, $\lambda = 0.633\,\mu$m, $n_S = 1.34$ and $n_P = 1.41$. In appendix A, we recall the results of the Lorentz-Mie calculation, and give a few details about the way in which the LM form factor was computed. Clearly the two form factors do not differ appreciably in the range of scattering angles where they take on significant values. The RG form factor severely deviates from the exact one at large angles, in a region of very low experimental signal to noise ratio. A short description of the experimental set up is given in the next section.

In conclusion, although the emulsions under study are always very turbid, we think our experimental conditions allow us to assume everywhere a single scattering regime and the applicability of the RG approximation.

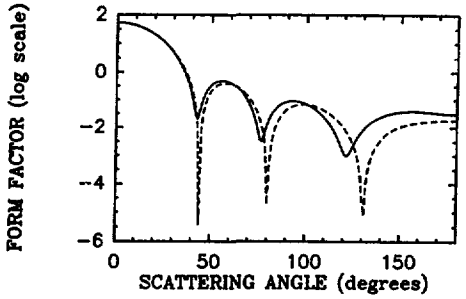

Fig. 6. — Comparison between the Lorentz-Mie and Rayleigh-Gans form factors for $\sigma = 0.93\,\mu$m ; $\lambda = 0.633\,\mu$m ; $n_s = 1.34$; $n_p = 1.41$.

4. Fluid phase and pair potential measurement.

In order to avoid multiple scattering, one way is to focus on very diluted systems, but in that case only the very small q vector range is sensitive to pair interactions. Unfortunately very small angle measurements are quite critical. An other approach consists in using more concentrated systems ($\Phi \sim 20\,\%$) in such a way that the structure factor is substantially

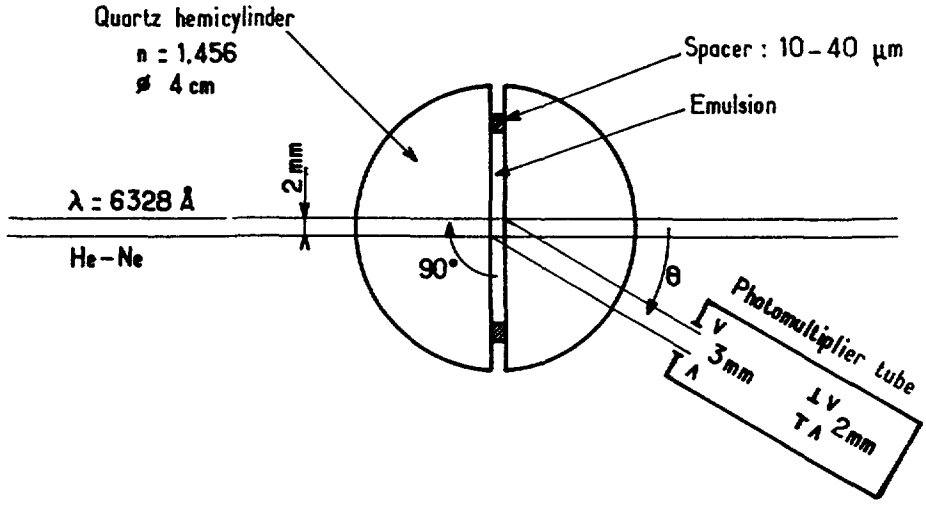

Fig. 7. — Experimental set up for static light scattering experiments on emulsion fluid phase.

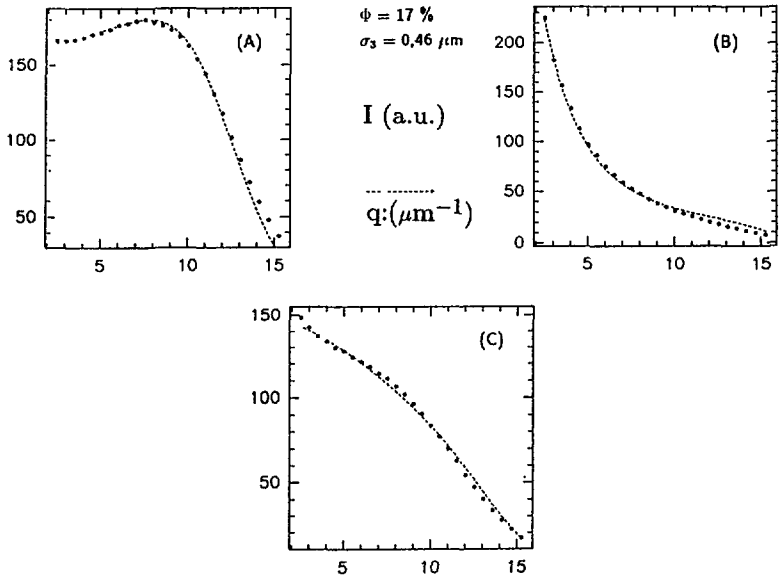

Fig. 8. — Scattering intensities *versus* wave vector in the fluid phase of the $\sigma = 0.46\,\mu$m, $\Phi = 0.17$ emulsion for three distinct situations. Points are experimental results and dotted lines are theoretical predictions (see text below) a) C = cmc ; $\Phi_m = 0$; $C_s = 0$; b) $C = 0.055$ mol.l^{-1} , $\Phi_m = 0.012$, $C_s = 0$; c) $C = 0.055$ mol.l^{-1} , $\Phi_m = 0.012$; $C_s = 0.2$ mol.l^{-1}

affected by interactions for larger angles. As seen above, multiple scattering can be avoided using very thin samples (20 μm). We used the set up shown in figure 7. The emulsion is contained between two quartz hemicylinders (4 cm in diameter).

The relatively high volume fraction of the emulsion, and thus the strong scattering of the

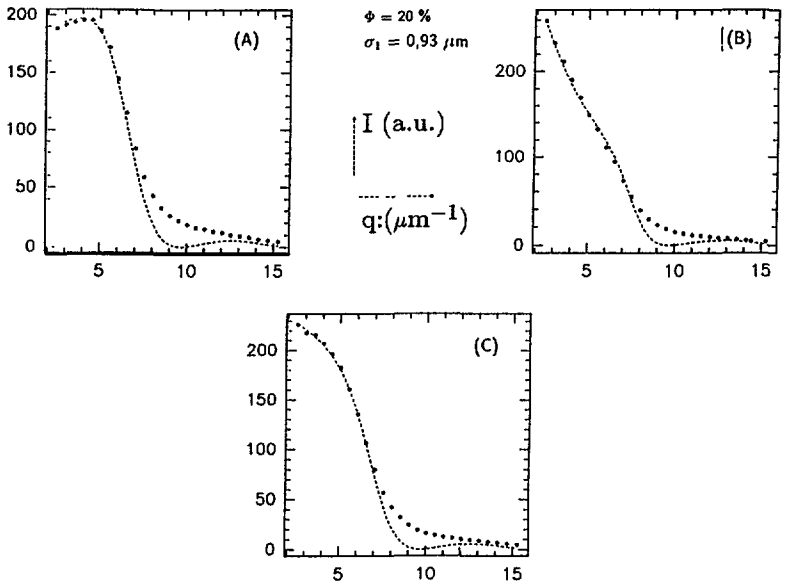

Fig. 9. — Scattered intensities *versus* wave vector in the fluid phase of the $\sigma = 0.93$, $\Phi = 0.2$ emulsion for three distinct situations. Points are experimental results and dotted lines are theoretical predictions (see text below) a) C = cmc , $\Phi_m = 0$, $C_s = 0$; b) $C = 0.025$ mol.l^{-1} , $\Phi_m = 0.005$, $C_s = 0$; c) $C = 0.025$ mol.l^{-1} , $\Phi_m = 0.005$, $C_s = 0.2$ mol.l^{-1}. Note that the theoretical form factor goes to zero for q close to 10 μm^{-1} which is not reproduced by experimental data. This can be attributed to the residual polydispersity or the presence of dust.

colloidal fluid ensures to make the scattering of droplets negligible compared to the one arising from the colloidal fluid. Notice that the small objects (micelles) responsible for the attractive interactions give rise to a negligible scattering compared to the one arising from the much bigger oil droplets. Up to now, direct measurements of depletion interaction using light scattering have been already attempted [16]. But in that case, polymers (responsible for the depletion interaction) have a scattering comparable with the one arising from the colloidal fluid. Such a situation complicates a lot the analysis in contrast with our experiment. Typical scattering data $I(q)$ as a function of the wave vector q are shown in figure 8 ($\sigma = 0.46\,\mu$m, Φ =17 %) and in figure 9 ($\sigma = 0.93\,\mu$m, Φ =20 %). The dots correspond to experimental data and the dotted lines are fits (see below). The labels (a), (b), and (c) refer to three distinct situations which illustrate the main effects of surfactant and salt concentrations. For the detailed concentrations see the figure captions. Let us just comment the general trends. Figure 8a and 9a correspond to a surfactant concentration (C) equal to the cmc and a salt concentration (C_s) equal to 0 mol.l^{-1} The emulsion exhibits in each case a correlation peak evoking the hard sphere behavior. The peak position goes to small q as the droplet diameter increases when the volume fraction is kept constant. This tendency is classical for such a fluid. Figure 8b and 9b correspond to a surfactant concentration just below the one corresponding to the phase transition. The salt concentration is still kept zero. As it is expected for a fluid with attractive interactions, compressibility fairly increases. This trend is still true for the three samples whatever the droplet size is and remains quite spectacular.

Figure 8c and 9c correspond to a surfactant concentration identical to the preceding case but for a salt concentration equal to 0.2 mol.l^{-1} This salt concentration corresponds to the

maximal extension of the reentrant fluid phase (see phase diagram Fig. 4b). In each case adding salt decreases the compressibility and changes the curvature of $I(q)$ towards a less attractive-like profile. This result is in accordance with the observed melting of the solid phase for added salt.

In order to interpret quantitatively our light scattering data we followed the same scheme as Huang *et al* [26]. Indeed, a quantitative study of the interaction is possible, fitting theoretical structure factors to the experimental curves. The theoretical structure factor is obtained using the mean spherical closure approximation which leads to an analytical form for $S(q)$ if the pair potential is taken to be a square well potential [26]. Three parameters define the square well potential: σ the hard sphere diameter, ϵ the depth of the potential, and r which defines the range of the potential as $\sigma(r-1)$. The diameter σ is precisely measured by analysing the solid Bragg diffraction patterns (see below). Since informations on both the depth and the range of the potential require very small q vector data analysis, we have to fix one parameter (our experiment does not approach the small angle domain). So the range of the square well potential is kept constant and taken to be the micellar diameter according to our depletion mechanism hypothesis. Finally the only free parameter is the depth of the potential which is extracted from the fit.

The theoretical scattering intensity is expressed by equation (3.1):

$$I(q) = \alpha \cdot P(q) \cdot S(q) \tag{4.1}$$

assuming the Rayleigh-Gans approximation to be valid.

– α is a non relevant parameter which is independent of q ; since we do not perform absolute measurements the α parameter could not have any physical meaning.

– $P(q)$ is completely defined (σ is known).

– $S(q)$ is calculated according to Sharma *et al.*'s equation [27], (see appendix 2). Then, following the Huang *et al.* improvement [26] to the Sharma *et al.'s* equation, the fitted square well depth is renormalized according to the equation:

$$\epsilon'/kT = \mathrm{Ln}\,(\epsilon/kT + 1) \tag{4.2}$$

Where ϵ' is the renormalized square well depth which will be only considered further.

In figures 8 and 9, dotted lines are fits of (4.1) to the experimental data. When the micelle volume fraction is equal to zero (i.e., surfactant concentration close to cmc) a background attraction is measured. The measured depth increases when the droplet diameter increases ($\sigma = 0.46\,\mu$m , $\beta\epsilon \simeq -1$; $\sigma = 0.6\,\mu$m , $\beta\epsilon \simeq -2$, $\sigma = 0.93\,\mu$m , $\beta\epsilon \simeq -3$). When the surfactant concentration is adjusted just below the phase transition threshold (Figs. 8b, 9b) we get a square well depth close to 4.5 kT, whatever the sample ($\sigma = 0.46\,\mu$m $\beta\epsilon \simeq -4.6$; $\sigma = 0.6\,\mu$m : $\beta\epsilon \simeq -4.8$; $\sigma = 0.95\,\mu$m : $\beta\epsilon \simeq -4.5$). As expected, the very strong modification of $I(q)$ when surfactant is added can be related to attractive interaction.

To support the micelles depletion mechanism hypothesis, we measured the interaction as a function of surfactant concentrations, (without salt) when one approaches the phase transition threshold. This experiment was performed on the intermediate size sample: ($\sigma = 0.60\,\mu$m, $\Phi = 17\,\%$). The measured square well depth ϵ increases linearly with Φ_m (the micelle volume fraction). This behavior confirms the depletion mechanism [28].

Concerning the salt effect, we can definitely conclude that salt decreases the depth of the potential when the same range of the potential is assumed. We measured a decay of $1\,kT$ for each sample when 0.2 mole.l^{-1} in salt is added to the fluid phase at the phase transition threshold (Figs. 8c, 9c). As previously noticed (Sect. 2) this result is in contradiction with

a DLVO picture. We suggest one plausible mechanism of such an effect on the depletion mechanism basis. The Debye length (κ^{-1}) is always negligible compared to the droplet diameter but remains of the same order of magnitude as σ_m, the ionic micellar diameter. So, we can expect that since the effective volume of micelles is involved, consequencies on depletion may occur. More precisely, when salt is added, κ^{-1} decreases and consequently the effective micelle volume decreases also, then the depletion interaction should decrease. Nevertheless quantitative estimates of this effect are not easy. The main problem is the calculation of the effective volume as a consequence of a screening effect. An other possible interpretation consists in evoking the SDS micelles size and shape modification with added salt but this effect remains quite small [29].

5. Dense phase: evidence for colloidal crystal structure.

The first indication for a solid structure (long range order) comes from observations under microscope of the dense phase separated by gravity (Fig. 3). Nevertheless, it could not be taken as a proof because a clear observation of the pure dense phase needs to constrain it between glasses (separated by few microns) which orientates the first reticular plane parallel to the glass plate. In order to characterise the colloidal crystal nature we collected the Bragg reflections diffracted by the cream. The dense phase is deposited between two parallel quartz plates kept 15 μm apart. This cell is located in a large (15 cm) cylindrical container filled up with brine which has exactly the same refractive index as the dense phase. Such a set up (see Fig. 10) allows us to choose both the area to be illuminated and the angle between incident beam and plates without modifying the scattering angles. The expected reticular distances require to use a 4880 Å Ar^+ laser and to cover the 10°-130° angular range, what corresponds to $1 - 30\,\mu m^{-1}$ wave vector range. For a check, we used a test sample : a calibrated bidimensional ($p = 1.8\,\mu m \pm 0.05$) lattice is located between glasses instead of the true sample and the corresponding Bragg reflexions are recovered. No artefact are disclosed: first and second order peaks are found with less than 2 % error compared with the predicted angles values, which are of the same order the ones expected in our experiments.

The diffraction peaks for the three samples are shown in figure 11. Two Bragg diffractions are collected but the small angle one is much more intense than the large angle one as expected from the form factor dependance on q. Indeed, to make visible the second peak, the incident intensity is largely enhanced. From Bragg equation and peaks positions we found corresponding reticular distances (see Tab. I) d_1 and d_2 with $d_1 > d_2$. The value of the ratio d_1/d_2 suggests a fcc structure for the colloïdal crystal. In such a case d_1 should correspond to the 111 plane (the dense plane) and d_2 to the 220 plane. Nevertheless the actual absence of the 200 fcc line suggests also a random-stacked mixture of both fcc and hexagonal close-packed. This result is similar to what found Pusey *et al.* [30] in a different system made of nearly hard spheres. Since the droplet-droplet distance is similar in the two lattices, the diameter may be accurately measured:

$$\sigma = \sqrt{3/2}\, d_{111} \tag{5.1}$$

and is taken to be the hard sphere diameter.

6. Fluid-solid phase transition with attractive potentials.

Fluid-solid phase transitions have been investigated by various authors. The hard sphere system exhibits a first order F.S. transition [31] leading to a fcc structure [30]. For purely

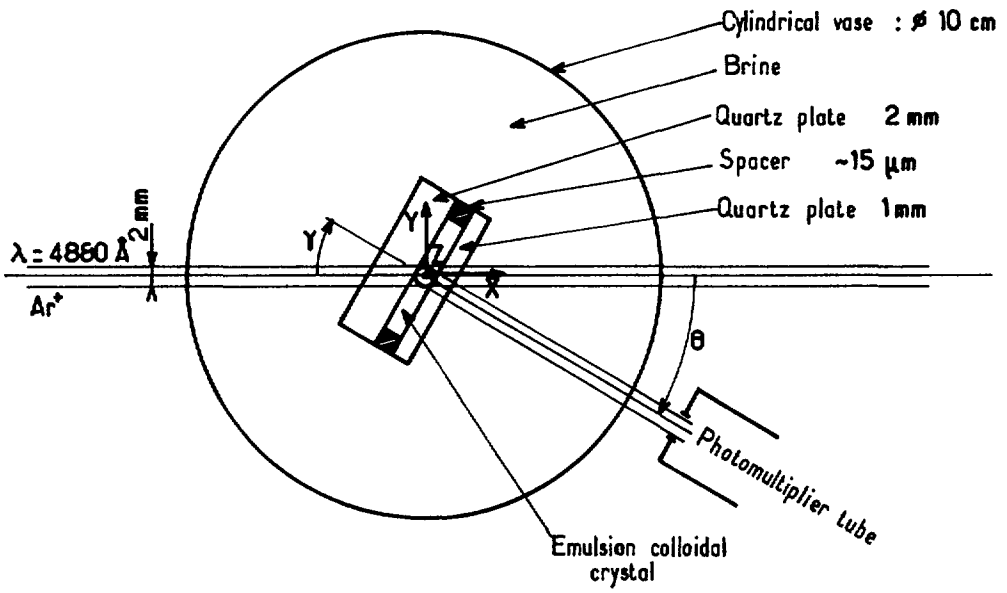

Fig. 10. — Experimental set up for Bragg diffraction experiments on oil droplet colloïdal powder.

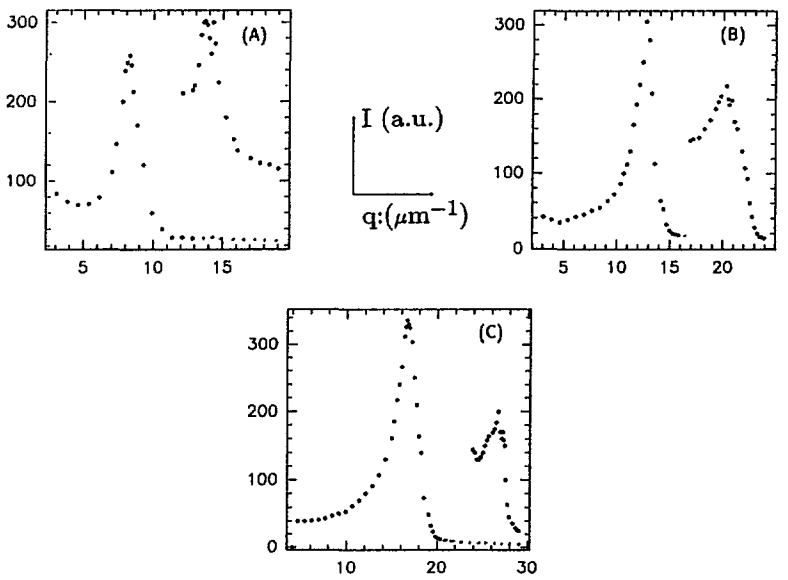

Fig. 11. — Diffracted intensities *versus* wave vector in the solid phase. Two diffraction peaks are found for each sample (a: $\sigma = 0.93\,\mu$m ; b: $\sigma = 0.6\,\mu$m ; c: $\sigma = 0.46\,\mu$m) which are compatible with a fcc structure.

repulsive systems experimental results [32, 33] on charged latex particles and theoretical calculations [34] indicate the possibility for both bcc and fcc structure depending on the parameters

Table I. — *Reticular distances measured from Bragg peak positions and deduction of the hard sphere diameters.*

	$\frac{d_1}{\mu m}$	$\frac{d_2}{\mu m}$	$\frac{d_1}{d_2}$	$\frac{\sigma}{\mu m} = \sqrt{\frac{1}{2}}\, d_{111}$
σ_1	0.758	0.462	1.64	0.928
σ_2	0.494	0.305	1.62	0.605
σ_3	0.377	0.231	1.63	0.461

of the screened interaction. For attractive hard sphere systems liquid-gas equilibria have been most often reported [35, 36]. Fluid-solid equilibrium was only suggested [17] but never characterized. However, some theoretical investigations of such transitions have been performed [37, 38]. One of them [37], using perturbation theory and the Vrij equation [8] for the pair potential, provides different scenari for the perturbation of the hard spheres transition. If the small objects diameter involved in the depletion potential is less than $\sigma/3$, then the liquid gas equilibrium is replaced by a fluid-solid equilibrium, which means that triple point disappears. Our aim is to propose an analytical approach of this transition in the dilute regime part of the phase diagram which can be considered as an extreme simplification of the work of Gast *et al.* [37] or Vincent *et al.* [38].

6.1 THERMODYNAMICS. — Taking into account that the fluid phase is dilute ($\Phi < 20\,\%$) and the solid phase mostly incompressible and compact (fcc structure, $\Phi = 74\,\%$) we worked out the following model: The fluid free energy density is taken to be the ideal gas one, which means that second order term involving the second virial coefficient is negligible compared to the entropic perfect gas contribution. This idea will be developped further.

The fluid partition function for a classical non ideal fluid is expressed as:

$$Z = \frac{\lambda^{-3N}}{N!} Q \tag{6.1}$$

where λ is the thermal wavelength defined as $\lambda = \left(\frac{2\pi\hbar^2}{m\,kT}\right)^{1/2}$ with $\hbar$ the Planck constant, kT the thermal energy and m the mass of a particle; N is the total number of particles; Q is defined as:

$$Q = \int \cdot \int \exp - \beta U\ (\mathbf{r}_1 \cdot\cdot\ \mathbf{r}_N)\ \mathrm{d}\mathbf{r}_1 \cdot\cdot\ \mathrm{d}\mathbf{r}_N \tag{6.2}$$

For an ideal gas the total potential energy is equal to zero. Then the equation (6.1) becomes:

$$Z = \frac{\lambda^{-3N}}{N!} V^N \tag{6.3}$$

where V is the total volume.

The free energy density f is given by:

$$f = \frac{F}{V}$$

with

$$F = -kT \operatorname{Ln} Z \tag{6.4}$$

$$f_G = kT\left(n\,\mathrm{Ln}(n\lambda^3) - n\right) \tag{6.5}$$

with $n = \dfrac{N}{V}$, the particle density.

Introducing the volume fraction variable defined as $\Phi = \dfrac{nv}{V}$ with v, the volume of one particle, we get:

$$f_G = \frac{kT}{v}\left(\Phi\,\mathrm{Ln}\,\Phi - \Phi + \Phi\,\mathrm{Ln}\,\frac{\lambda^3}{v}\right) \tag{6.6}$$

This expression can be rewritten as:

$$f_G = \frac{kT}{v}\left(\Phi\,\mathrm{Ln}\,\Phi + \Phi\left(\mu_G^0 - 1\right)\right) \tag{6.7}$$

where μ_G^0 is the dimensionless reference chemical potential for the ideal gas:

$$\mu_G^0 = \mathrm{Ln}\,\frac{\lambda^3}{v} \tag{6.8}$$

The solid free energy is derived from Einstein model, H being the total energy per particle in the lattice :

$$H = \frac{P^2}{2m} + \frac{1}{2}m\,\omega_0^2 < x^2 > + U_0 \tag{6.9}$$

where P is the impulsion; ω_0, the Einstein frequency; $< x^2 >$, the mean square deplacement; U_0, the lattice energy.

For the solid phase, the partition function is:

$$Z = z^N \tag{6.10}$$

with

$$z = h^{-3}\int \cdot \int \mathrm{e}^{-\beta H}\,\mathrm{d}\mathbf{r}\,\mathrm{d}\mathbf{p} \tag{6.11}$$

Solving the Gaussian integrals gives:

$$z = \left(\frac{kT}{\hbar\,\omega_0}\right)^3 \mathrm{e}^{-\beta U_0} \tag{6.12}$$

The solid free energy density can be extracted:

$$f_S = n_S\,kT\left(\beta U_0 - 3\,\mathrm{Ln}\,\frac{kT}{\hbar\omega_0}\right) \tag{6.13}$$

Introducing the Φ variable and the solid reference chemical potential μ_S^0, in (6.13) gives:

$$f_S = \frac{kT}{v}\,\Phi_S\left(\beta U_0 + \mu_S^0\right) \tag{6.14}$$

with:

$$\mu_S^0 = -3\,\mathrm{Ln}\,\frac{kT}{\hbar\omega_0} \tag{6.15}$$

6.2 PHASE DIAGRAMS. — We describe a strongly first order phase transition where the two phases in equilibrium have a very different composition, one is very dilute (liquid phase) and the other is very concentrated and mostly incompressible (solid phase). We can assume that the solid phase has a constant volume fraction Φ_S. Consequently, we assume a very deep and sharp minimum for the solid free energy density, this will drastically simplify the classical demixtion equations. Instead of two equations (equal pressure and equal chemical potential in each phase) [39] we are left with:

$$f_G + (\Phi_S - \Phi)\frac{df_G}{d\Phi} = f_S(\Phi_S) \tag{6.16}$$

This equation gives the oil volume fraction Φ in the fluid phase, in equilibrium with a solid phase (constant volume fraction Φ_S) at the freezing point.

Using the equations (6.7) and (6.14) we can solve (6.16) and get:

$$\beta U_0 = \mathrm{Ln}\,\Phi - \Phi/\Phi_S + (\mu_G^0 - \mu_S^0) \tag{6.17}$$

with:

$$\mu_G^0 - \mu_S^0 = 3\,\mathrm{Ln}\left(\frac{\lambda}{v^{1/3}\hbar\omega_0}\right) \tag{6.18}$$

Besides, the lattice energy U_0 can be expressed (using Eq. (2.2)) as:

$$\beta U_0 = -\frac{z}{2}\left(\frac{3}{2}\Phi_m\frac{\sigma}{\sigma_m} + w\right) \tag{6.19}$$

where w is the Van der Waals contribution to the lattice energy and z the nearest neighbours number for a fcc structure ($z = 12$). The equation (6.19) is of course a crude approximation because the lattice energy of the dense crystal is calculated using the pair potential of equation (2.2) which works in principle only at infinite dilution. It is clear that a more exact approach would be to treat this problem as a compressible binary fluid made of big and small spheres. Nevertheless we propose here the simplest analytical model which will compare quite well with experiments.

Combining (6.17) and (6.19), and neglecting the linear terms (Φ/Φ_S), we obtain:

$$\Phi_m = \frac{\sigma_m}{9\sigma}\left(-\mathrm{Ln}\,\Phi + (\mu_S^0 - \mu_G^0) - 6w\right), \tag{6.20}$$

which is the phase boundary equation in the (Φ, Φ_m) plane. This is a two parameters description of the phase diagram of the form:

$$\Phi_m = A(-\mathrm{Ln}\,\Phi + B) \tag{6.21}$$

providing a logarithmic behavior with $A = \dfrac{\sigma_m}{9\sigma}$ and $B = \mu_S^0 - \mu_G^0 - 6w$. Notice that this treatment leads to separate the depletion contribution (A) from the poorly unknown contributions due to the solid entropy and lattice Van der Waals energy.

The parameters A and B are then extracted from a fit to the experimental phase diagram (Fig. 4a). The results are listed in table II. It is clear that the logarithmic behavior provided by our simple Ideal Gas-Harmonic Solid approach agrees very well with the experiments. In view of the crudness of our model, the quantitative agreement of the depletion parameter A with the theoretical value provided by the perfect gas depletion hypothesis (Eq. (2.1)) can be

Table II. — *Experimental values of the parameter A and B deduced from the fit. The parameter A compares quantitatively well with the theoretical prediction* $\frac{\sigma_m}{9\sigma}$ *based on a depletion mechanism hypothesis.*

	$\frac{\sigma_m}{9\sigma}$	A exp	B exp
$\sigma = 0.93\,\mu m$	$4 \times 8\,10^{-4}$	$11 \times 5\,10^{-4}$	3.0
$\sigma = 0.6\,\mu m$	$7 \times 5\,10^{-4}$	$11 \times 5\,10^{-4}$	6.7
$\sigma = 0.46\,\mu m$	$9 \times 5\,10^{-4}$	$18 \times 5\,10^{-4}$	5.2

considered as satisfying. Note that with two different methods, light scattering experiments and phase diagram analysis, we find the same agreement with a micelle depletion mechanism.

The experimental value of the parameter B is also in agreement with what is expected. Using Lindmann criterium for melting [40], the mean square displacement is taken to be $(\sigma/\alpha)^2$ where α is equal to 10. Then, combining with the classical equipartition energy theorem : $\frac{3}{2} kT = \frac{1}{2} m\omega_0^2 \left(\frac{\sigma}{\alpha}\right)^2$, the equation (6.18) becomes:

$$\Delta\mu^0 = \mu_G^0 - \mu_S^0 = \mathrm{Ln}\left(\left(\frac{2\pi}{3}\right)^{3/2} \frac{6}{\pi} \alpha^{-3}\right) \tag{6.22}$$

$\Delta\mu^0$ is equal to 7 when α is choosen to be 10 [40]. If the Van der Waals contact energy w is taken to be of the order of $1kT$, then we get B close to 1 which is of the same order of magnitude than what is extracted from the fit.

7. Discussion.

Interactions have been measured by light scattering analysis, but at the same time an ideal gas behavior is required to describe the F – S phase transition, even for relatively high oil volume fraction. The ideal gas behavior is demonstrated by the logarithmic shape of the F – S phase boundary. Let us now discuss the physical reasons of such a result using very simple analytical arguments. Finally we will be able to give a physical understanding of the appearance conditions for a triple point.

Very early, Long *et al.* [41] recognized the possibility for a colloidal dispersion to reach a thermodynamical equilibrium state where two phases are coexisting. This equilibrium was qualitatively interpreted evoking a Boltzmann relationship of the type: $\Phi = \Phi_f \exp - \frac{\beta U_0}{kT}$, where U_0 is the depth of the attractive pair potential (originaly, the DLVO secondary minimum), Φ and Φ_f are respectively the volume fractions of the particles in the fluid phase and in the flocculated phase, β is the average number of contacts of a surface particle in a floc. Later, Vincent *et al.* [42] gave a theoretical basis to this empirical law using a lattice gas approach. On the basis of the work of Gast *et al.* [37] who first introduced theoretically the Fluid-Solid phase transition hypothesis, Fleer *et al.* [43] derived a logarithmic law for the transition of the form $\Phi_f = \Phi_S \exp\left(\frac{\beta U_0 + C(\Phi_S)}{kT}\right)$ very similar to ours. The $C(\Phi_S)$ term is an empirical

correction for the excluded volume of the particles in the solid like (floc) phase. Recently the validity of such an equation was tested by Vincent *et al.* [38] on more accurate (calculation) basis. It was concluded that the logarithmic behavior for the gas solid like phase boundary in fact is valid only in the limit of very dilute dispersions ($\Phi < 0.1\,\%$). We will discuss in more details the validity of the logarithmic law and the required conditions for a fluid-solid transition instead of a liquid-gas transition.

Let us start with the virial expression for the fluid phase free energy:

$$f_F = \frac{kT}{v}\left(\Phi \operatorname{Ln}\Phi + \Phi\left(\mu_G^0 - 1\right) + \frac{B}{v}\Phi^2 + \frac{C}{v^2}\Phi^3 + \cdot\right) \tag{7.1}$$

where B is the second virial coefficient defined as:

$$B = -2\pi \int_0^\infty \left(e^{-u(r)/kT} - 1\right) r^2\, dr \tag{7.2}$$

$u(r)$ being the pair potential and where C is the third virial coefficient which depends mostly on the hard sphere contribution to the pair potential. Assuming a square well pair potential, we obtain an analytical form for the coefficient B :

$$\frac{B}{v} = 4 - 4\left(e^{-\beta\epsilon} - 1\right)\cdot\left(\lambda^3 - 1\right) \tag{7.3}$$

where $\beta\epsilon$ and λ are defined as in section 4:

$$\lambda = 1 + \frac{\delta}{\sigma},$$

δ being the range of the square well potential.

Considering the virial expansion we will just discuss how this function is modified when the droplet size is increased for a given square well potential. The trivial consequence is that the ratio $\frac{\delta}{\sigma}$ goes to zero, and the second virial coefficient remains equal to the hard sphere part which is equal to 4. Consequently the negative second order contribution disappears and a fluid-fluid demixtion becomes impossible. Moreover, the free energy of such a big droplet fluid is ideal gas like as long as the second order hard sphere contribution is negligible compared to the ideal gas logarithmic term. This approximation might be still valid for a droplet volume fraction equal to ten percents. In that case, the gas-solid phase boundary equation is the one derived in section 6 which exhibits the logarithmic behavior:

$$\beta U_0 = \operatorname{Ln}\Phi + \Delta\mu^0 \tag{7.4}$$

Now we consider how this simple equation is modified when the second order contribution in the virial expansion is taken into account.

Solving equation (6.16) we get a first order correction to the logarithmic background:

$$\beta U_0 = \operatorname{Ln}\Phi + 2\frac{B}{v}\Phi + \Delta\mu^0 - \frac{\Phi}{\Phi_S} \tag{7.5}$$

Consequently a linear term is added to the logarithmic term which can be either positive or negative depending on the ratio δ/σ discussed above.

Let us examine now how a critical point associated to a liquid-gas equilibrium may appear. Using the virial expansion and assuming the third virial coefficient $\frac{C}{v^2}$ equal to 5 as it is commonly admitted [23] we can deduce the required values of Φ and $\frac{B}{v}$ to get à L-G critical point. It cómes:

$$\begin{aligned} \frac{B_c}{v} &\simeq -5 \\ \Phi_c &\simeq 0.18 \end{aligned} \tag{7.6}$$

Again, notice that such a value for $\frac{B}{v}$ can not be reached if the ratio δ/σ is very small, and consequently the critical point can be absent. The boundary between the situation with a $F-S$ transition only and the critical point appearance corresponds to the superposition of the triple point and the critical point. Such a condition is achieved if the $F-S$ demixtion equation is satisfied for $\Phi = \Phi_c$.

$$f(\Phi_c) + (\Phi_S - \Phi_c) \left.\frac{df}{d\Phi}\right)_{\Phi_c} = f_S(\Phi_S) \tag{7.7}$$

Combining (6.14) and (6.1) with (7.7) we obtain:

$$\beta\epsilon^* = \frac{2}{z\Phi_S}\left[(2b_c\Phi_S - 1)\Phi_c + (3c\Phi_S - b_c)\Phi_c^2 - 2c\Phi_c^3 + \Phi_S \mathrm{Ln}\,\Phi_c + \Phi_S(\mu_G^0 - \mu_S^0)\right] \tag{7.8}$$

with:

$$b_c = \frac{B_c}{v} \quad \text{and} \quad c = \frac{C}{v^2}$$

This equation gives the minimal value of the depth of a square well potential (ϵ^*) which leads to a fluid-solid phase transition for $\Phi = \Phi_c$ and $B = B_c$ (superposition of critical and triple point). Solving equation (7.3) we deduce the onset value for the parameter λ ($\lambda = 1 + \delta/\sigma$), which is:

$$\lambda^* = \left(1 + \frac{1 - \frac{B_c}{4v}}{e^{-\beta\epsilon^*} - 1}\right)^{1/3} \tag{7.9}$$

Consequently, the parameter which governs the phase diagrams topology for a one component fluid interacting *via* a square well pair potential is the ratio δ/σ. For small values of δ/σ the fluid-solid transition is expected only, whereas for higher values the liquid-gas transition is first preferred as it is illustrated in figure 12.

Numerical calculations [37] lead to the value $\delta/\sigma \simeq \frac{1}{3}$ for a one component fluid interacting *via* a depletion interaction (Eq. (2.1)). The same order of magnitude is found using this analytical approach when reasonable parameters are introduced in equation (7.8) ($\frac{B_c}{v} = -5$, $C = 5$, $\Delta\mu_0 = 7$, $\Phi_c = 0.18$, $\Phi_S = 0.6$).

Finally we conclude that emulsions which are big droplets colloids ($\sigma \sim 1\,\mu$m) feature only a $F-S$ transition. Since the attractive interaction is induced by a micelle depletion mechanism, the ratio δ/σ (which is equal in that case to $\frac{\sigma_m}{\sigma}$) is always very small and the logarithmic shape for the phase transition is expected as long as excluded volume effect in the fluid phase can be neglected.

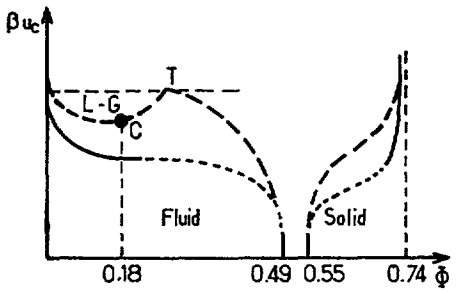

Fig. 12. — Phase diagrams in the $\beta u_c/\Phi$ plane. For $\beta u_c = 0$ the only one phase transition accessible is the hard sphere transition (u_c is the contact pair potential) *If* $\beta u_c \neq 0$ two distinct scenari are possible according to the value of the ratio δ/σ: (range of the pair potential δ over particle diameter σ).

8. Conclusion - summary.

We have demonstrated the role of surfactant dissolved in the continuous phase of an oil in water emulsion. The interaction mechanism can be described according to the perfect gas model proposed by Vrij on the basis of the Asakura and Oosawa depletion hypothesis. This resulting attractive depletion interaction leads to a fluid-solid phase transition only. The F – S phase boundary is logarithmic and no fluid-fluid transition occurs, due to the very small value of the ratio $\frac{\sigma_m}{\sigma}$ where σ_m is also the range of the attractive interaction. The colloidal crystals resulting in that phase transition have a fcc structure with an irridescent cream appearance. The reentrant fluid phase induced by added salt can be qualitatively interpreted on the basis of an effective micellar diameter which is reduced by salt. Consequently the depletion pair potential becomes less attractive and the solid melts. Finally, the very well known creaming effect of emulsions is a fluid-solid transition induced by surfactant micelles but the polydispersity masks the colloidal crystal character of the aggregates in usual industrial polydisperse emulsions.

Acknowledgements.

The authors thank P. Bothorel, P. Peignier and G. Schorsch for introducing them to emulsion science. They are very grateful to F. Nallet and C. Coulon for fruitful discussions on many aspects of statistical mechanics. They would like also to thank J.R. Lalanne and P. Méléard for their help in optic and image analysis. This work has been supported in part by Rhône-Poulenc Compagny France.

Appendix 1.

Mie scattering.

In the experimental conditions defined in paragraph 4, namely an incident field $\mathbf{E}_0$ perpendicular to the scattering plane, the light scattered by a single sphere of radius a is polarized in the same direction as $\mathbf{E}_0$, and its amplitude is given by the Lorentz-Mie solution [24]:

$$E_S = \frac{iE_0}{k_0 R} e^{-ik_0 R} S(\theta) \qquad \text{(A1.1)}$$

R, the distance between the sphere and the detector, is supposed to be large compared to λ.

$S(\theta)$ is an infinite series:

$$S(\theta) = \sum_{n=1}^{\infty} \frac{2n+1}{n(n+1)} \left[\alpha_n \pi_n(\cos\theta) + \beta_n \tau_n(\cos\theta)\right] \tag{A1.2}$$

with π_n and τ_n given by:

$$\pi_n(\cos\theta) = \frac{1}{\sin\theta} P_n^1(\cos\theta) \tag{A1.3a}$$

$$\tau_n(\cos\theta) = \frac{\mathrm{d}}{\mathrm{d}\theta} P_n^1(\cos\theta) \tag{A1.3b}$$

where $P_n^1(n)$ are associated Legendre functions. The coefficients α_n and β_n are given by:

$$a_n = \frac{\varphi_n'(y)\,\varphi_n(x) - m\,\varphi_n(y)\,\varphi_n'(x)}{\varphi_n'(y)\,\xi_n(x) - m\,\varphi_n(y)\,\xi_n'(x)} \tag{A1.4}$$

$$b_n = \frac{m\,\varphi_n'(y)\,\varphi_n(x) - \varphi_n(y)\,\varphi_n'(x)}{m\,\varphi_n'(y)\,\xi_n(x) - \varphi_n(y)\,\xi_n'(x)} \tag{A1.5}$$

with the following notations:

$$x = k_0\, a \qquad y = \frac{n_S}{n_P}\, x \tag{A1.6}$$

φ_n and ξ_n are Riccati-Bessel functions.

In practice, the $S(\theta)$ expansion can be reliably restricted to the order n equal to the integer nearest to x. This simplification is a consequence of the "localization principle" [24]. In the situations of concern in this study, we have computed the LM form factors up to the sixth order terms in (A1.2).

Appendix 2.

Equation for the structure factor.

The analytical equation obtained by Sharma [27] and Sharma for a fluid interacting *via* a square well potential is the following one:

$$S(q) = \frac{1}{1 - C(q)} \tag{A2.1}$$

with $C(q)$ given by:

$$\begin{aligned} C(q) = -\frac{24\eta}{(q\sigma)^6} \{ & \alpha(q\sigma)^3[\sin q\sigma - q\sigma\cos q\sigma] \\ & + \beta(q\sigma)^2\left[2q\sigma\sin q\sigma - (q^2\sigma^2 - 2)\cos q\sigma - 2\right] \\ & + \gamma\left[(4q^3\sigma^3 - 24q\sigma)\sin q\sigma - (q^4\sigma^4 - 12q^2\sigma^2 + 24)\cos q\sigma + 24\right] \\ & - (\epsilon/kT)(q\sigma)^3[\sin\lambda q\sigma - \lambda q\sigma\cos\lambda q\sigma + q\sigma\cos q\sigma - \sin q\sigma]\} \end{aligned} \tag{A2.2}$$

where α, β, γ are given by:

$$\alpha = \left[(1+2\eta)^2 + n^3(\eta-4)\right]/(1-\eta)^4 \tag{A2.3}$$

$$\beta = -\frac{1}{3}\eta\left(18+20\eta-12\eta^2+n^4\right)/(1-\eta)^4 \tag{A2.4}$$

$$\gamma = \frac{1}{2}\eta\left[(1+2\eta)^2 + n^3(\eta-4)\right]/(1-\eta)^4 \tag{A2.5}$$

η is given by the equation:

$$\eta = \pi n \sigma^3/6 \tag{A2.6}$$

where n is the number density of particles and σ the particle diameter. ϵ, and λ are the parameters defining the depth and the range of the square well potential.

References

[1] LISSANT K.J., Emulsion and emulsion technology, **6**, (M. Dekker, New York, 1974).
[2] BECHER P., emulsions; theory and practice, (Rheinhold, New York, 1965).
[3] COCKBAIN E., *Trans. Faraday Soc.* **4** (1952) 185.
[4] HIGUCHI W., OKADA R., LEMBERGER A., *J. Pharm. Sci.* **51** (1962) 683.
[5] FAIRHURST D., ARONSON M., GUM M., GODDARD E., *Colloids Surf.* **7** (1983) 153.
[6] ARONSON M.P., *Langmuir* **5** (1989) 494.
[7] ASAKURA S., OOSAWA F., *J. Chem. Phys.* **22** (1954) 1255.
[8] VRIJ A., *Pure Appl. Chem.* **48** (1976) 471.
[9] JOANNY J.F., LEIBLER L. and DE GENNES P.G., *J. Polymer Sci. Polymer, Phys. Ed.* **17** (1979) 1073.
[10] SPERRY P.R., *J. Coll. Int. Sci.* **99** (1984) 97.
[11] SPERRY P.R., HOPFENBERG H.B., THOMAS N.L., *J. Coll. Int. Sci.* **82** (1981) 62.
[12] MA C., *Colloids Surf.* **28** (1987) 1.
[13] DE GENNES P.G., *C.R. Acad. Sc. Paris* **t.292** (1991).
[14] ATTARD P., *J. Chem. Phys.* **91** (1989).
[15] ADJARI A., PELITI L., PROST J., submitted to *Phys. Rev. Lett.* (1991).
[16] DE HEK H. and VRIJ A., *J. Colloid Int. Sci.* **88** (1982) 258.
[17] GAST A.P., RUSSEL W.B., HALL C.K., *J. Coll. Int. Sci.* **109** (1986).
[18] BIBETTE J., accepted to *J. Coll. Int. Sci.* (1991).
[19] PEIGNIER M., Rhône Poulenc Company, 69191 St-Fons (France).
[20] VERWEY E.J.W., OVERBEEK J.F.G., Theory of the stability of lyophobic colloids, (Elsevier, Amsterdam, 1948).
[21] PASHLEY R.M., NINHAM B.W., *J. Phys. Chem.* **91** (1987) 2902.
[22] VINCENT B., CLARKE J., BARNETT K.G., *Colloids Surf.* **17** (1986) 65.
[23] HANSEN J.P., MACDONALD I.A., Theory of simple liquids, (Academic Press, New York, 1976).
[24] VAN DE HULST H.C., Light scattering by small particles, (Wiley, New York, 1957).
[25] KERKER M., The scattering of light, (Academic Press, New York, 1969).
[26] HUANG S., SAFRAN S.A., KIM M.W., GREST G.S., KOTHARCKY K.M., QUIRKE N., *Phys. Rev. Lett.* **53** (1984).
[27] SHARMA R.V., SHARMA K.C., *Physica* **89A** (1977) 213.
[28] BIBETTE J., ROUX D., NALLET F., *Phys. Rev. Lett.* **65** (1990) 2470.
[29] MISSEL J.P., MAZER N.H., BENEDEK G.B., CAREY M.C., *J. Phys. Chem.* **87** (1983) 1264.
[30] PUSEY P.N., VAN NEVEN W., BARTLETT P., ACKERSON B.J., RARITY J.G., UNDERWOOD S.M., *Phys. Rev. Lett.* **63** (1989) 2753.

[31] ALDER B.J., HOOVER W.G., YOUNG D.A., *J. Chem. Phys.* **49** (1968) 3688.
[32] WILLIAMS R., CRANDALL R.S., *Phys. Lett.* **48A** (1974) 225.
[33] PIERANSKY P., *Contemp. Phys.* **24** (1983) 25.
[34] CHAIKIN P.M., PINCUS P., ALEXANDER S., *J. Coll. Int. Sci.* **8ç** (1982) 255.
[35] PATHMAMANOHARAN C., DE HEK H., VRIJ A., *Coll. Polym. Sci.* **259** (1981) 769.
[36] JANSEN J.W., DE KRUIF C.G., VRIJ A, *J. Coll. Int. Sci.* **114** (1986).
[37] GAST A.P., HALL C.K., RUSSEL W.B., *J. Coll. Int. Sci.* **96** (1983) 251.
[38] VINCENT B., EDWARDS J., ENNETT S., CROOT R., *Coll. Surf.* **31** (1988) 267.
[39] ANDELMAN D., CATES M.E., ROUX D., SAFRAN S.A., *J. Chem. Phys.* **87** (1987) 7229.
[40] BERRY R.S., RICE S.A., ROSS J., Physical Chemistry, **891** (Wiley, 1976)
[41] LONG J.A., OSMOND D.W.J., VINCENT B., *J. Coll. Int. Sci.* **42** (1973) 545.
[42] VINCENT B., CUCKHAM P.F., WAITE F.A., *J. Coll. Int. Sci.* **73** (1980)
[43] FLEER G.J., SCHENTJENS J.M.H.M., VINCENT B., *ACS Symp. Ser.* **240** (1984) 245.